RESEARCH PAPER

on the High Temperature Compressive Flow Behavior of Mg-4Sn Magnesium Alloy

Ata Abdi, Mehrdad Aghaie-Khafri*

* *maghaei@kntu.ac.ir*
Materials Processing Lab, Faculty of Materials Science and Engineering, KN Toosi University of Technology, Tehran, Iran

Received: January 2021 **Revised: September 2021** **Accepted: December 2021**

DOI: 10.22068/ijmse.2085

Abstract: *Hot deformation behavior of homogenized Mg-4Sn binary alloy was studied using compression tests in the temperature range of 300-500°C and strain rates of 0.001-1s^{-1}. The material showed typical single peak flow behavior followed by a steady state flow as a plateau, which was more evident at the high value of Zener-Hollomon parameter. Constitutive analysis showed that in spite of the original Johnson-Cook (J-C), conventional strain compensated Arrhenius model based on the Sellars-McTegart model, had a reasonable agreement with the experimental data. Moreover, the well-known hyperbolic sine function fitted the experimental data for predicting of the peak stress with a fair degree of accuracy.*

Keywords: *Magnesium alloys, Microstructure, Hot deformation, Constitutive model.*

1. INTRODUCTION

Cast magnesium alloys have gained more popularity in recent years due to their ability to maintain high strengths at light weights. Magnesium offers unique properties and has gained widespread usage as components and structural applications in the automotive industry, and non-automotive applications such as computer, electronics and power tool industries. Magnesium alloys usage is continuing to expand due mainly to that they are 35% lighter than aluminum alloys and 78% lighter than steel [1]. The interest in Mg-Sn based alloys started in the early 1930s [2, 3]. However, after 2000 there has been an increased global demand in these alloys which are believed to have potential for structural applications at elevated temperatures.

According to the binary phase diagram [4], the solubility of Sn in Mg decreases from 14.85 wt.% at the eutectic transformation temperature of 561°C to less than 0.45 wt.% at 200°C. The intermetallic phase Mg_2Sn in Mg-Sn alloys has a high melting point (770°C) and known as a thermally stable intermetallic precipitate [5]. It has been shown that the formation of fine thermally stable Mg_2Sn particles is the main strengthening mechanism in these alloys mainly due to that they distributed at the boundaries of the as-cast Mg-Sn alloy. Moreover, this phase can be easily precipitated as a result of high solubility limit (about 3.35 atomic.pct) [6].

Even though Mg alloys typically exhibit comparable ductility to other light alloys, the low temperature formability is severely limited, and a number of researchers are seeking to develop alloys and thermomechanical processing schemes to improve the forming performance. Generally, formability of HCP metals is less than other cubic metals due to fewer available slip systems at room temperature. According to von Mises more than 5 independent slip systems must operate in polycrystals to deform uniformly and to prevent failure at the grain boundaries. Magnesium is close packed hexagonal, and there are no five independent slip systems. Consequently, it is necessary that other non-basal slip systems are activated or deformation occurs by twinning [7]. However, activation of additional slip systems at increased temperatures allows large elongation and makes them comparable with other cubic metals. The deformation mechanisms involve slip, twinning, grain boundary sliding and cavitation.

In the recent years, a comprehensive study has been done on the creep resistance behavior and age hardening response of as-cast and as-extruded Mg-Sn based alloys. Yungui Chena et al. [4] revealed that the Mg-5Sn alloy is the one exhibiting the best tensile properties at room temperature among the Mg-xSn (x= 1, 3, 5, 7, 10) alloys. O. Sallary et al. [8] extract the processing map of the Mg-Sn alloy through hot compression tests. Based on Do Hyang Kim et al. [9] creep

[DOI: 10.22068/ijmse.2085]

resistance remarkably improves with the presence of Mg_2Ca phase. The Mg_2Ca phase changed the fracture behavior from inter-granular to trans-granular fracture mode. Mg_2Ca precipitates show higher thermal stability against coarsening than Mg_2Sn precipitates. Xiaoping Luo et al. [10] investigated high-temperature deformation behaviors of the as-cast Mg-Sn-Y-Zr alloy at 250 to 450°C and 0.002 to 2 s^{-1} strain rates. They proposed that the apparent activation energy of the as-cast Mg-Sn-Y-Zr alloy was 223.26 kJ /mol and the stress exponent was 9.7.

Despite the efforts made to establish the Mg-Sn alloys behavior, there is still work to be done to experimentally analyze the hot deformation behavior of the Mg-4Sn binary alloy. Therefore, the aim of this research is to investigate hot deformation characteristics of the Mg-4Sn alloy.

2. MATERIALS AND METHODS

2.1. Casting and homogenizing

The raw materials used for casting were 99.9% pure magnesium, 99.9% pure tin alloy. Melting was carried out in an electrical furnace under the Argon+SF_6 covering flux to protect the molten magnesium from oxidation. The melt was held at 700°C for 15 min and mechanically stirred for 3 min before Sn was added to it. Then, melt was poured into a permanent mold preheated to 200°C. Chemical composition of the cast material obtained by the inductively coupled plasma (ICP) method is listed in Table 1. The cast bars had dimensions of 35 mm diameter and 180 mm length. The cast alloy was homogenized at 475°C for 5 h.

2.2. Hot compression test

The compression specimens were machined from the homogenized bars into cylinders with a length of 12mm and a diameter of 8mm. Hot compression tests were conducted using a Zwick Roell 250 testing machine (Zwick GmbH & Co. KG, Ulm, Germany), equipped with a fully computerized furnace. Hot compression was carried out at temperatures of 300°C, 350°C, 400°C, 450°C and 500°C and strain rates of 0.001 s^{-1}, 0.01 s^{-1}, 0.1 s^{-1} and 1 s^{-1}. The compression specimens were heated to the deformation temperature and held for 5 min prior to compression in order to ensure a uniform temperature along the specimen and elimination of any thermally gradient. The specimens were immediately water quenched after compression to save the compressed microstructure.

In each test, the load-stoke data were converted into the true stress-true plastic strain data after making corrections for friction using the following equation [11]:

$$\frac{P}{\sigma}=\left(\frac{h}{4\mu a}\right)^2\left(e^{2\mu a/h}-\frac{2\mu a}{h}-1\right) \quad (1)$$

where σ is the friction corrected flow stress, P the uncorrected flow stress, a and h are instantaneous radius and height of the specimen and μ is the friction coefficient which was determined according to the amount of the barreling for each specimen [12].

3. RESULTS AND DISCUSSION

3.1. Stress-strain curve

The true stress-true strain curves of compressed Mg-4Sn alloy at different strain rates and deformation temperatures are shown in Fig. 1. It is clear that the flow stress level depends on the deformation temperature and strain rate. Stress-strain curves at low temperature and high strain rate, high Zener-Hollomon parameter, show a peak stress followed by a continuous decrease in the flow stress. However, at high temperature and low strain rate, low Zener- Hollomon parameter, the flow stress reached steady state at strains greater than about 0.3. Such a behavior has been reported by other researchers [13, 14]. It is interesting to note that in magnesium polycrystals, prismatic and pyramidal slips are activated above 225°C and 350°C, respectively [15]. Variations of the peak stress as a function of temperature and strain rate are shown in Fig. 2. Fig. 2 (a) reveals that the peak stress decreases by increasing of temperature at a given strain rate.

Table 1. Chemical composition of the cast alloy in wt%

Ba	Fe	Mn	K	Na	Sn	Mg	Rest
0.0132	0.0192	0.0239	0.282	1.81	4.271	93.55	0.0307

[DOI: 10.22068/ijmse.2085]

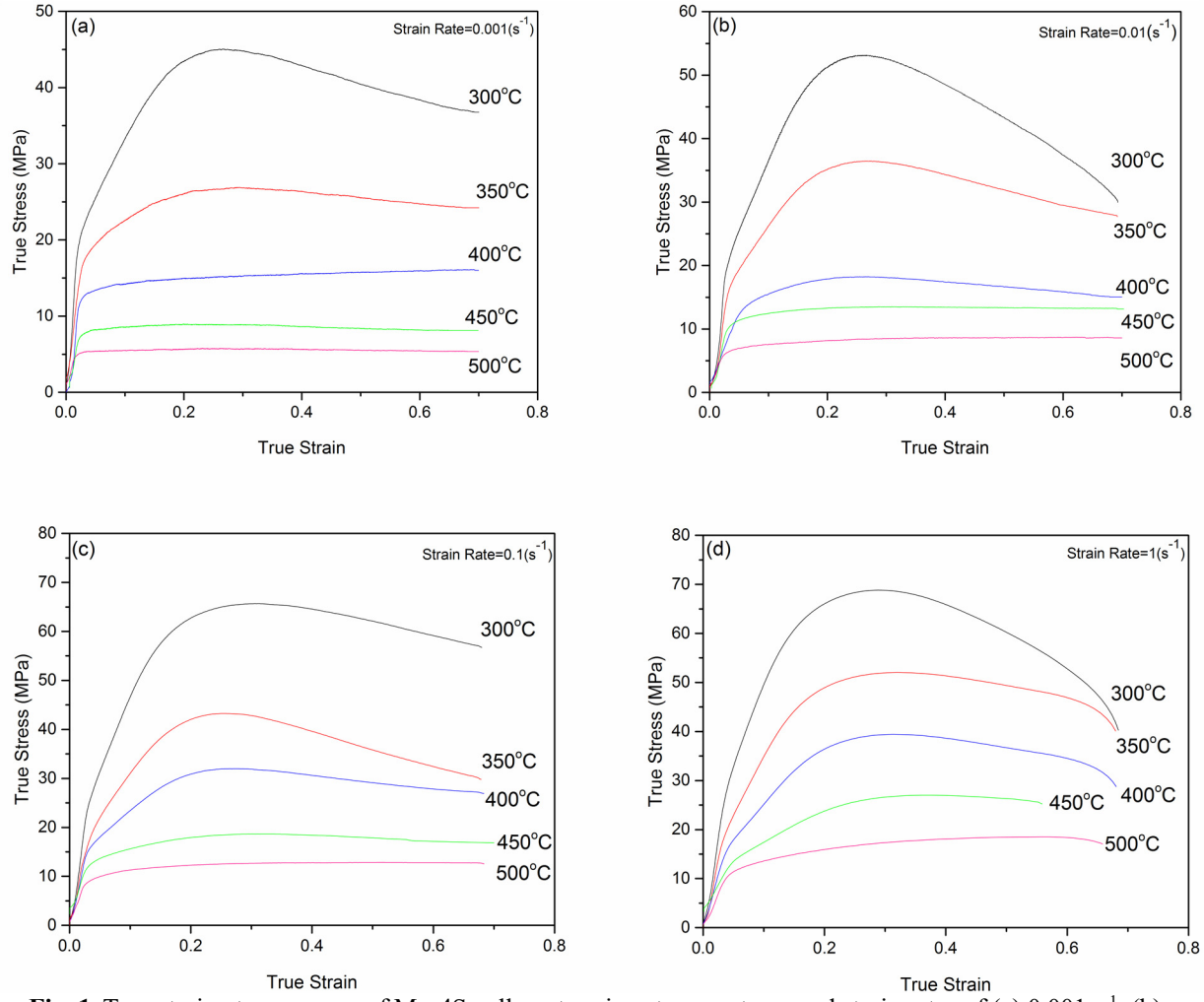

Fig. 1. True strain-stress curves of Mg-4Sn alloy at various temperatures and strain rates of (a) 0.001 s^{-1}, (b) 0.01 s^{-1}, (c) 0.1 s^{-1} and (d) 1 s^{-1}.

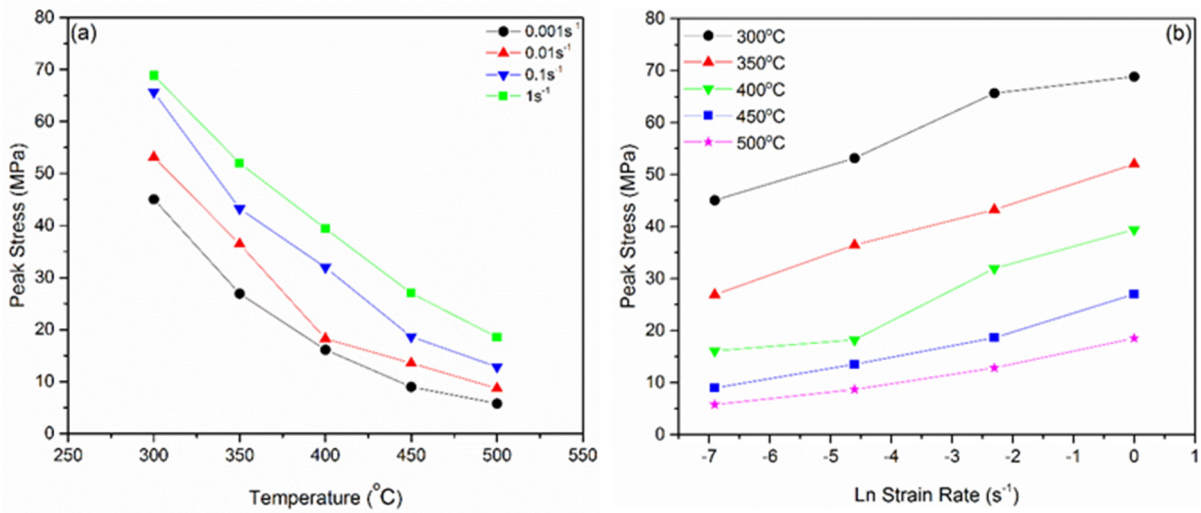

Fig. 2. Peak stress as a function of (a) temperature, (b) strain rate.

[DOI: 10.22068/ijmse.2085]

It has been reported that high temperatures decrease the required critical resolved shear stress for activating of basal and non-basal slip systems (prismatic and pyramidal), and promote dislocation climb and cross slip [16-19].
However, the slip-twinning transition temperature for this alloy is around 250°C and the major contribution of the pyramidal and prismatic slip systems at high temperatures (>300°C) definitely suppress the deformation twin formation. Fig 2 (b), shows the increase of peak stress by increasing of the strain rate at a given temperature. This can be attributed to the generation of higher dislocation density caused by increasing of strain rate and accumulation of strain. At high strain rate the deformation time is decreased and dynamic recrystallization (DRX) is postponed.
It is interesting to note that at strain rate of 0.001 s^{-1} and temperature range 450-500°C, the sharp peak in the flow stress curve disappears and a plateau is observed. The difference between the peak stress and the minimum stress is most significant in the temperature range of 300- 400°C. It is well known that at low values of the Zener-Hollomon parameter, dislocation mobility at grain boundaries increased as well as annihilation or rearrangement of dislocation; thus, nucleation or growth of recrystallized grains occurred more easily.

3.2. Constitutive models

The primary goal of establishing a constitutive model is to predict the flow stress and describe the plastic deformation behavior during the hot deformation [20]. Phenomenological models are mostly used to predict the flow stress by considering the effect of temperature and strain rate. In this study, different phenomenological models including Johnson-Cook, Arrhenius-type and strain compensated are considered.

3.2.1. Johnson-Cook model

The Johnson-Cook (J-C) constitutive model is a phenomenological model in which the effects of temperature, strain rate and strain on the flow stress are considered. The original Johnson-Cook model is widely used for aluminum and steel, but there are few available studies on the magnesium alloys. The J-C constitutive equation can be represented as [21-27]:

$$\sigma = \left(\sigma_o + K\varepsilon^n\right)\left(1 + C\ln\dot{\varepsilon}^*\right)\left(1 - T^{*q}\right) \quad (2)$$

where σ is flow stress, Ɛ represents strain, $\dot{\varepsilon}_o$ is dimensionless strain rate and can be shown as $\dot{\varepsilon}^* = \dot{\varepsilon}/\dot{\varepsilon}_o$ where $\dot{\varepsilon}_o$ is strain rate and $\dot{\varepsilon}_o$ is the reference strain rate. T* stands for homologous temperature which can be expressed as $T^* = \left(T - T_r\right)/\left(T_m - T_r\right)$, where T indicates the absolute deformation temperature, T_m is melting temperature (650°C for Mg-4Sn alloy) and T_r is the reference temperature ($T_r \leq T$). Moreover, σ_0 is the proof stress at the reference strain rate and reference temperature which is calculated at a strain value of 0.002 [28]. K is the coefficient of the strain hardening, *n* is the strain hardening exponent, C and q are the material constants which represent the coefficient of the strain rate hardening and thermal softening exponent, respectively.
Determination of n and K: In order to calculate the material's constants n and K, $\dot{\varepsilon}_o$ and T_r are taken as 0.001s^{-1} and 300°C, respectively. It is interesting to note that incorporating reference condition in Eq. (1) results in a Ludwik type equation. Fig. 3 shows the relationship between $\ln(\sigma-\sigma_o)$ and Lnε at the reference strain rate and temperature. The slop and intercept of the fitting line represents the strain hardening exponent (n) and Ln k values, respectively.

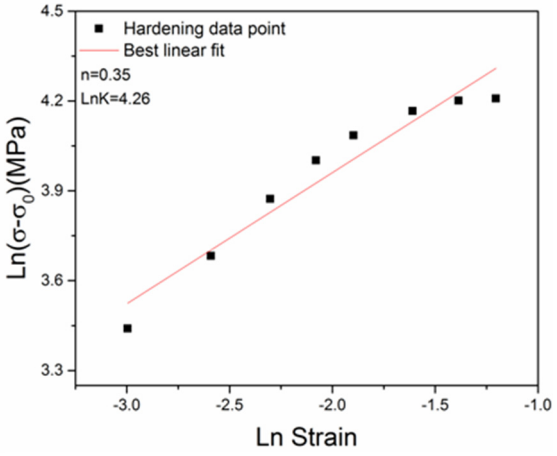

Fig. 3. Relationship between $\ln(\sigma-\sigma_o)$ and Lnε at reference strain rate and temperature.

Determination of C: To calculate the C constant, which is the strain rate hardening coefficient, Eq. (1) can be simplified by assuming T^* equal to zero (i.e. $T=T_r$):

[DOI: 10.22068/ijmse.2085]

$$\frac{\sigma}{\sigma_o + K\varepsilon^n} = 1 + C\ln\dot{\varepsilon} \quad (3)$$

The relationship between $\sigma/\sigma_0 K\varepsilon^n$ and $ln\dot{\varepsilon}$ at various range of strain (0.1-0.65) and strain rate at the reference deformation temperature is shown in Fig. 4. The average value of C constant has been calculated as 0.067.

Determination of q: The q constant refers to the thermal softening exponent. Another assumption, $\dot{\varepsilon} = \dot{\varepsilon}_r$, has been made to evaluate q. This makes the second parenthesis in Eq. (2) to be disappeared:

$$\sigma = \left(\sigma_o + K\varepsilon^n\right)\left(1 - T^{*q}\right) \quad (4)$$

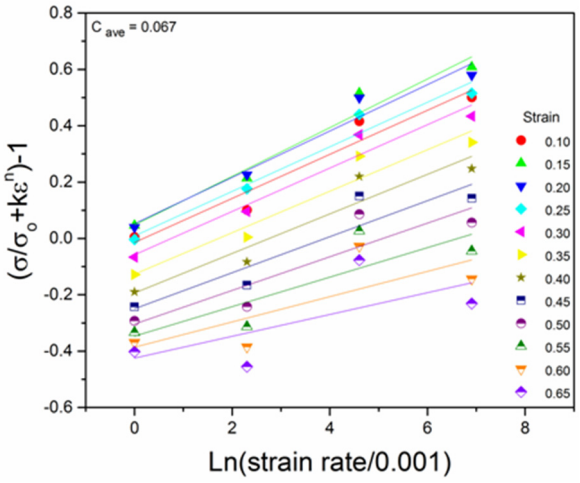

Fig. 4. Plot of $\frac{\sigma}{\sigma_o + K\varepsilon^n}$ vs. $ln\dot{\varepsilon}$ at reference condition.

Fig. 5 shows a plot of $\mathrm{Ln}(1-(\sigma/(\sigma_o + K\varepsilon^n))$ vs. LnT^* at given strain values of 0.1-0.65. The q constant value of 0.471 was obtained based on the average slope of fitted lines.

Stress−strain curves for compromising the experimental data and predicted flow stress by the J-C model are shown in Fig. 6. It can be observed that the J-C model provides reasonable results in the work hardening region of curves under various strain rates and temperatures. On the other hand, at high strain value poor agreement with the experimental results is observed, and the accuracy of the model is unacceptable. This contradicted behavior could be attributed to the intrinsic features of the J-C model in which any deformation history consisting of the thermal and strain rate history is neglected. Moreover, the effects of strain, strain rate and temperature are separately considered. There is a significant dependence of C and q values on strain at each mentioned condition. Unreasonable flow stress predictions of the J-C model have been reported by other researchers [29-33].

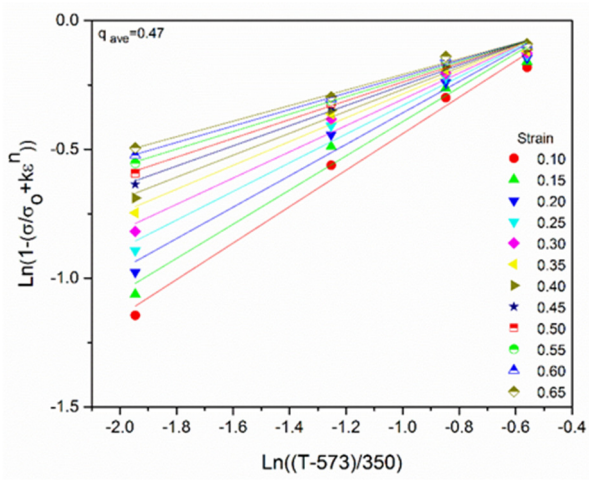

Fig. 5. Relationship between $\mathrm{Ln}(1-(\sigma/(\sigma_o + K\varepsilon^n))$ and LnT^*.

All material constants of equation (2) are summarized in Table 2. By substituting of these values, Eq. (2) can be simplified as follows:

$$\sigma = (1.45151 + 71.0313\varepsilon^{0.35128}) \times (1 + 0.0672217 Ln\frac{\dot{\varepsilon}}{0.001}) \times (1 - (\frac{T-573}{350})^{0.47110583}) \quad (5)$$

Table 2. Material constants of J-C model

n	K	C	q
0.35	71.03	0.07	0.47

3.2.2. *Arrhenius-type model*

The Arrhenius equation is widely used by researchers for predicting material's behavior at various strain rates and temperatures, especially the peak stress prediction. Moreover, the effects of temperature and strain rate on the deformation behavior may also be represented by the Zener-Holloman parameter (Z) in an exponent type equation [34]. The correlation between the flow stress, temperature and strain rate can be represented by the power law, the exponential law and the hyperbolic sine-type equation in low stress, high stress and all range of the stress levels, respectively:

[DOI: 10.22068/ijmse.2085]

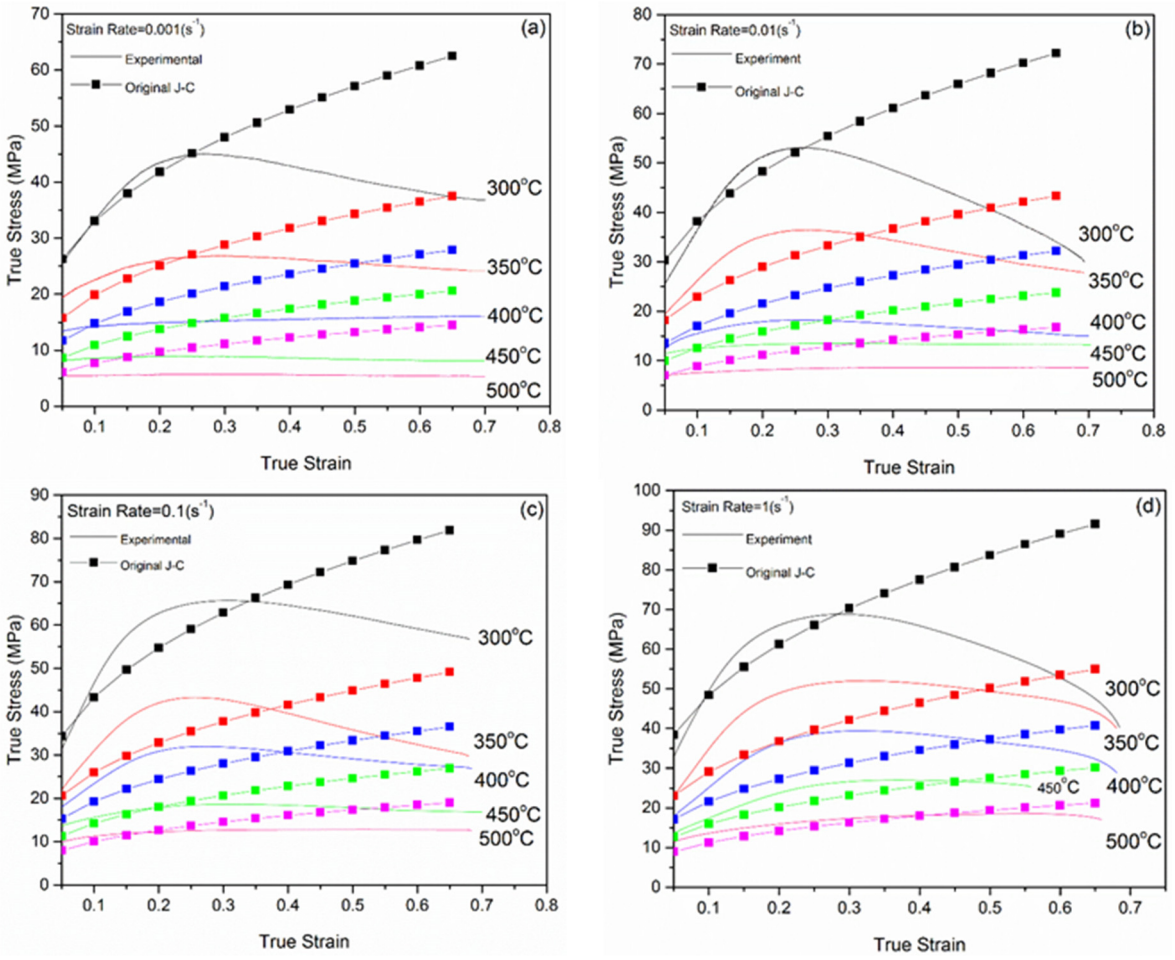

Fig. 6. Comparison between experiment and predicted flow stress by J-C model at different temperatures and strain rates of (a) 0.001 s^{-1}, (b) 0.01 s^{-1}, (c) 0.1 s^{-1} and (d) 1 s^{-1}.

$$Z = \dot{\varepsilon}\exp(\frac{Q}{RT}) = \begin{cases} A_1\sigma^{n1} \\ A_2\exp(\beta\sigma) \\ A\left[\sinh(\alpha\sigma)\right]^n \end{cases} \quad (6)$$

where Q is activation energy of deformation (kJ. mol^{-1}), R is the universal gas constant (8.314 J $mole^{-1}$ K^{-1}), T is the absolute temperature in K, $\dot{\varepsilon}$ is strain rate (s^{-1}) of the process. A, A_1, A_2, β, n1, α and n are materials constants, α= β /n1.

Power law model: To calculate constants A1 and n1, the power law equation could be expressed as follows:

$$\sigma_p = \left[\frac{1}{A1}\dot{\varepsilon}\exp(\frac{Q}{RT})\right]^{\frac{1}{n1}} \quad (7)$$

where n1 and Q can be defined as:

$$n1 = \left[\frac{\partial Ln\dot{\varepsilon}}{\partial Ln\sigma_p}\right]_T$$

or

$$\sigma_p = (\frac{Z}{A1})^{\frac{1}{n1}} \Rightarrow LnZ = LnA1 + n1Ln\sigma_p \Rightarrow$$

$$n1 = \left[\frac{\partial Ln\,Z}{\partial Ln\sigma_p}\right] \quad (8)$$

$$Q = Rn1\left[\frac{\partial Ln\sigma_p}{\partial(\frac{1}{T})}\right]_{\dot{\varepsilon}} \quad (9)$$

Considering Eq. (7), the values of n1 and A1 is obtained from the slope and intercept of LnZ vs. Ln peak stress (Fig. 7) as n1= 8.35 and LnA1= 20.05. The n1 constant also could be obtained from the mean slope values of Ln $\dot{\varepsilon}$ vs. Ln peak stress (Fig. 8), n1= 8.84.

[DOI: 10.22068/ijmse.2085]

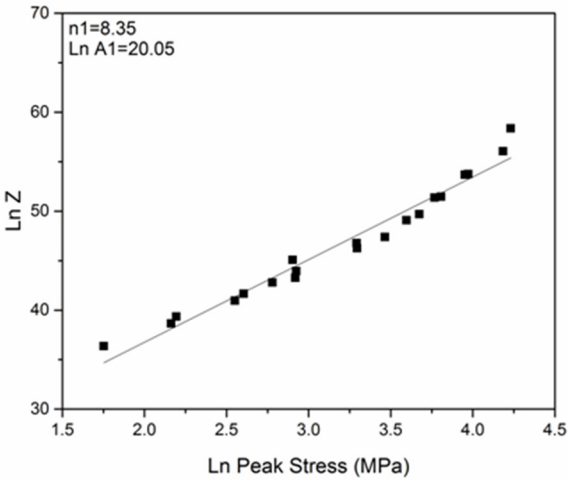

Fig. 7. The relationship between LnZ vs. Ln peak stress.

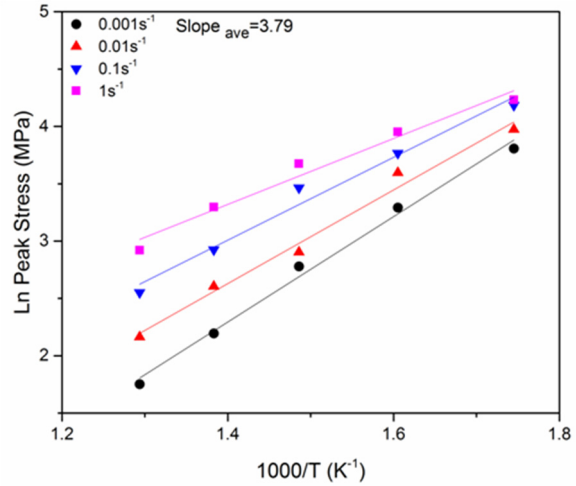

Fig. 9. The relationship between Ln peak stress vs. 1000/T at given strain rates.

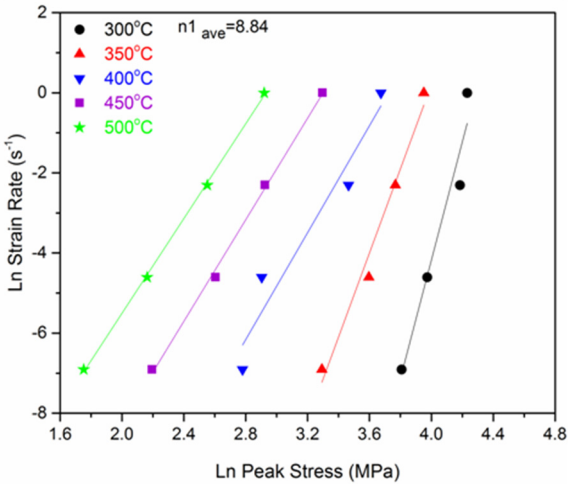

Fig. 8. The relationship between Ln &vs. Ln peak stress at given temperatures.

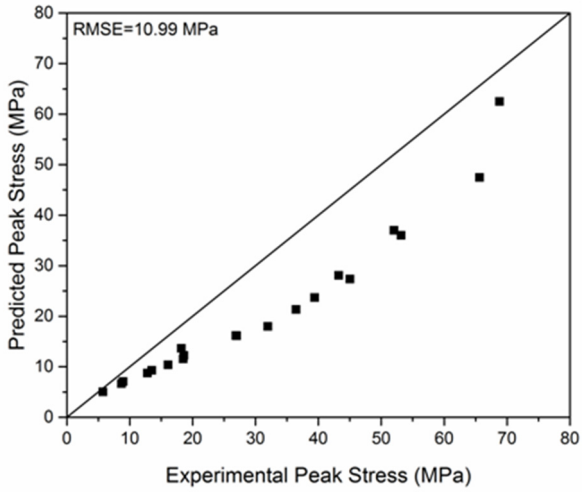

Fig. 10. The relationship between experimental and predicted peak stress based on the power law model.

Activation energy was calculated from the mean slope values of Ln peak stress vs. 1000/T, shown in Fig. 9, as Q= 263 kJ. mol^{-1}. By substituting all constants (n1, A1, Q) in Eq. (7), the power law equation for predicting the peak stress of Mg-4Sn alloy can be represented as follows:

$$\sigma_p = \left[\frac{1}{510040146.9}\&\exp\left(\frac{263000}{8.314T}\right)\right]^{\frac{1}{8.35}} \quad (10)$$

The correlation between the prediction of power law equation and the experimental peak stress for Mg-4Sn alloy is shown in Fig. 10. It can be observed that at high stress levels the prediction of the power law model is not reasonable. Frost and Ashby [35] used the power law for pure magnesium at 300°C and up to 80 MPa stress, but they reported that it is quite inaccurate for higher stress at elevated temperature.

Exponential Model: By using algebraic operations, Eq. (6) can be rewritten as follows:

$$\sigma_p = \frac{1}{\beta}\left\{Ln\left[\&\exp\left(\frac{Q}{RT}\right)\right] - LnA2\right\} \quad (11)$$

where β and Q can be defined as:

$$\beta = \left[\frac{\partial Ln\&}{\partial \sigma_p}\right]_T$$

Or

$$\sigma_p = \frac{1}{\beta}\mathrm{Ln}\left(\frac{Z}{A2}\right) \Rightarrow LnZ = LnA2 + \beta\sigma_p \Rightarrow \beta = \left[\frac{LnZ}{\sigma_p}\right] \quad (12)$$

$$Q = R\beta\left[\frac{\partial \sigma_p}{\partial\left(\frac{1}{T}\right)}\right]_{\&} \quad (13)$$

[DOI: 10.22068/ijmse.2085]

Considering Eq. (12), the values of β and A2 is obtained from the slope and intercept of LnZ vs. peak stress (Fig.11) as β= 0.328 and LnA2= 39.99. The β constant also could be obtained from the mean slope values of Ln $\dot{\varepsilon}$ vs. peak stress plot (Fig. 12) as β= 0.342.

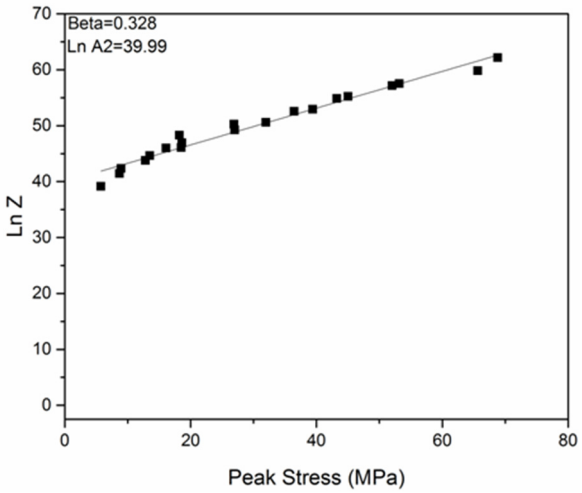

Fig. 11. The variation of LnZ vs. peak stress.

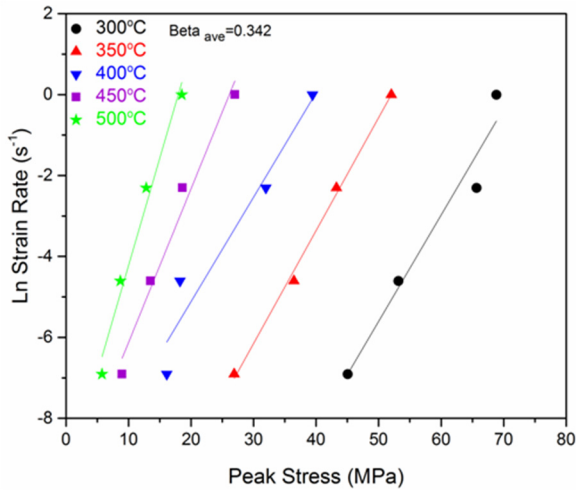

Fig. 12. The relationship between Ln $\dot{\varepsilon}$ vs. peak stress at given temperatures.

The activation energy can be calculated from the mean slope of the peak stress vs. 1000/T (Fig.13) which is equal to Q= 284 kJ. mol^{-1}. The value of α = β /n1 was also calculated as 0.039 MPa^{-1}.
By substituting all constants (β, A2, Q) in Eq. (11), the exponential equation for predicting the peak stress in Mg-4Sn alloy is:

$$\sigma_p = \frac{1}{0.328}\left\{Ln\left[\dot{\varepsilon}\exp\left(\frac{284000}{8.314T}\right)\right] - 39.99\right\} \quad (14)$$

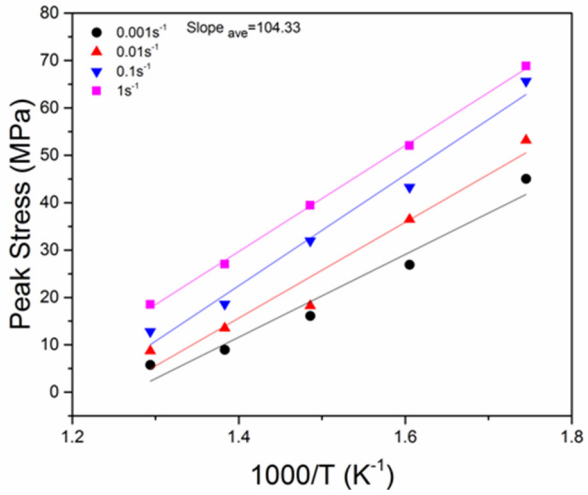

Fig. 13. The relationship between Ln peak stress vs. 1000/T at given strain rates.

Fig. 14 shows a poor correlation between the predicted and the experimental peak stress at high stresses. Sloof et al. [36] used an exponential law, but found it was not reasonable for slow strain rates and temperatures over 300°C.

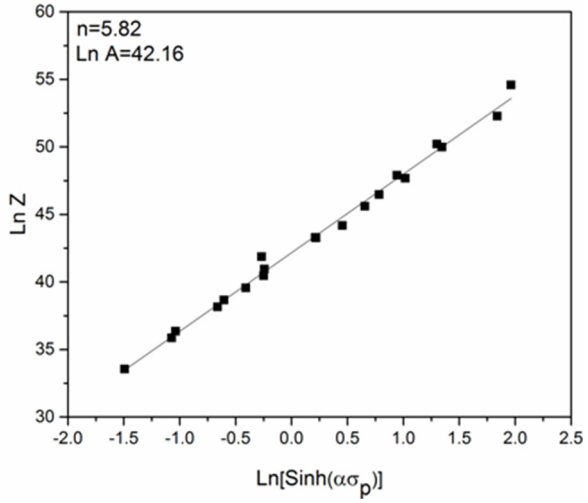

Fig. 14. Correlation between the experimental and the predicted peak stress based on the exponential model.

Hyperbolic sine-type Model: A hyperbolic sine-type equation has been used [37, 38] for a more precise approximation of the flow behavior using the Zener-Hollomon equation and flow stress.
A hyperbolic law combines an exponential and a power law to predict the flow behavior at various range of stress.
Eq. (6) can be rewritten as a function of the Zener-Hollomon parameter:

[DOI: 10.22068/ijmse.2085]

$$\sigma_p = \frac{1}{\alpha} Ln\left[(Z/A)^{1/n} + \sqrt{(Z/A)^{2/n} + 1} \right] \quad (15)$$

Then, the material's constants n and Q can be expressed as follows:

$$n = \left[\frac{\partial Ln\dot{\varepsilon}}{\partial Ln[\sinh(\alpha\sigma_p)]} \right]_T$$

or

$$Z = A\left[\sinh(\alpha\sigma_p)\right]^n \Rightarrow LnZ = LnA + nLn\left[\sinh(\alpha\sigma_p)\right]$$

$$n = \left[\frac{\partial LnZ}{\partial \mathrm{Ln}[\sinh(\alpha\sigma_p)]} \right] \quad (16)$$

$$Q = nR \left[\frac{\partial Ln[\sinh(\alpha\sigma_p)}{\partial(\frac{1}{T})} \right]_{\dot{\varepsilon}} \quad (17)$$

Considering Eq. (16), the slope and intercept of LnZ-Ln[sinh(ασp)] indicates n and A parameters, respectively, as shown in Fig. 15.

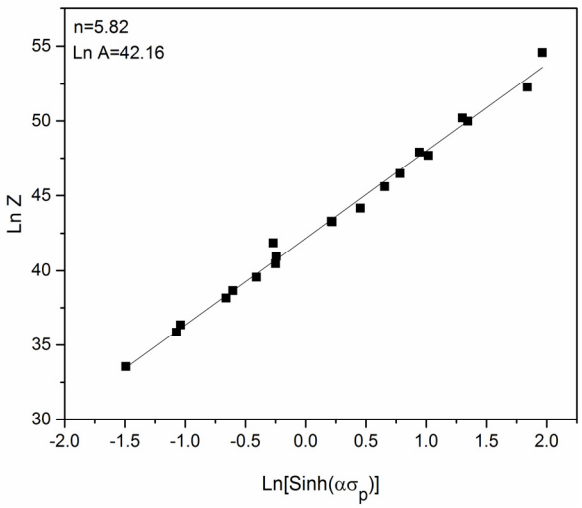

Fig. 15. Variation of LnZ as a function of Ln[sinh(ασp)].

The relationship between Ln[sinh(ασp)] and 1/T was used for evaluating the activation energy, as is shown in Fig. 16. The mean value of the activation energy was calculated as 260 kJ/mol. The calculated activation energy is greater than the activation energy for self diffusion in pure magnesium (135 kJ/mol). It can be attributed to the presence of Mg_2Sn phase in the Mg-Sn alloy system. It has been shown that Mg_2Sn phase precipitates along the grain boundaries and hinder the grain boundary migration and grain boundary sliding.

Following evaluating of all constants, the peak stress equation can be described using the Zener-Hollomon parameter as follows:

$$\sigma_p = \frac{1}{0.039} Ln\left[(Z/2.04106E+18)^{1/5.82} + \sqrt{(Z/2.04106E+18)^{2/5.82} + 1} \right] \quad (18)$$

$$Z = \dot{\varepsilon}\exp(\frac{260000}{8.314T})$$

Concerning Eq. (18), the predicted peak stress at a given strain rate and temperature can be calculated. Fig. 17 shows the relationship between experimental and predicted peak stress based on the hyperbolic sine-type model. It is clear that the hyperbolic sine-type model shows a very good agreement with the experimental results.

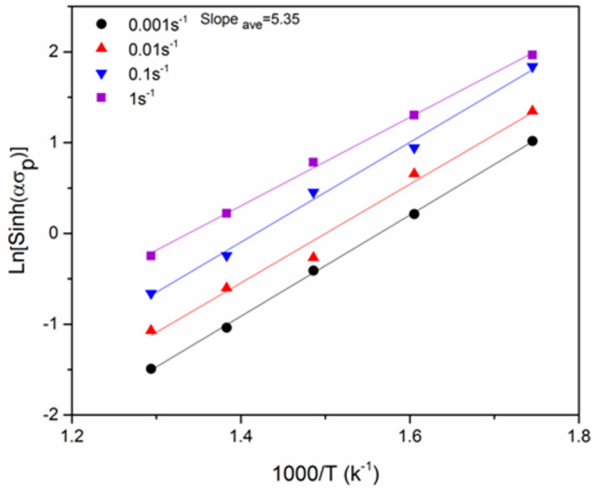

Fig. 16. Evaluating of activation energy from Ln[sinh(ασp)] vs. 1/T.

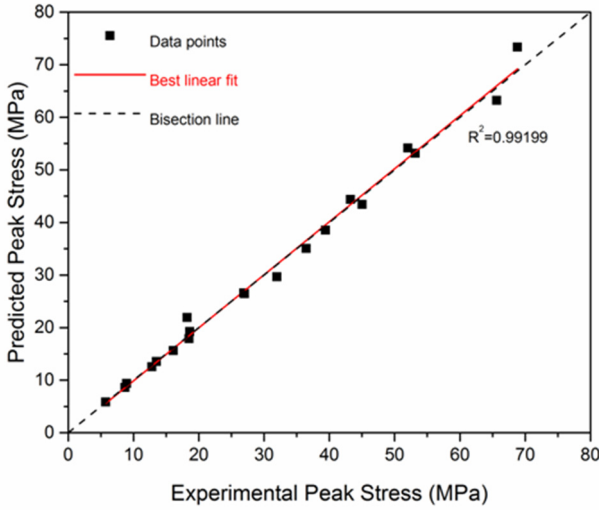

Fig. 17. The relationship between the experimental and the predicted peak stress based on the hyperbolic sine-type model.

[DOI: 10.22068/ijmse.2085]

3.2.3. *Comparison of phenomenological models*

The accuracy of different models was evaluated based on the root mean square error (RSME) and the average relative absolute error (AAE). RSME and AAE are defined as [38]:

$$RMSE = \sqrt{\frac{1}{N}\sum_{i=1}^{N}(t_i - y_i)^2} \quad (19)$$

$$AAE = \frac{1}{N}\sum_{i=1}^{N}\left|\frac{t_i - y_i}{t_i}\right| \times 100 \quad (20)$$

where t_i and y_i are experimental and calculated results, respectively. The calculated RSME and AAE for different models are listed in Table 3. It can be observed that the hyperbolic sine-type equation exhibits the least error and the highest precision in predicting the peak stress.

Table 3. Calculated RMSE and AAE for power law, exponential and hyperbolic sine-type models

Model	RMSE (MPa)	AAE (%)
Power law	10.99	30
Exponential	19.57	99
Hyperbolic sine-type	1.46	2.85

The capability of different models to predict the peak stress at temperatures out of the experimental ranges can be somehow assessed by RMSE and AAE. Generally, the models with low RMSE, i.e. hyperbolic sine model can be used for different temperatures in the range of 300-500°C. However, for temperatures below the slip-twinning transition temperature, about 250°C, the results of the models are less accurate due to the activation of twin assisted deformation mechanisms. The mean value of the activation energies based on the power law, exponential, and hyperbolic sine-type models were calculated as 263, 284, and 260 kJ/mol, respectively. The calculated activation energies are greater than the activation energy for self-diffusion in pure magnesium (135 kJ/mol). The reported apparent activation energy for different Mg-Sn alloys are as follows: Mg-8Sn-1.5Al: 153.5 kJ/mol, Mg-2Sn-2Ca: 183 kJ/mol, Mg-5Sn-2Ca: 198 kJ/mol [39-41]. The calculated activation energy for Mg-4Sn is higher than Mg-Sn base ternary alloys.

3.2.4. *Strain compensated Arrhenius-type model*

Considering the hyperbolic sine-type model, the effect of strain on the material constants for the hot deformation of Mg-4Sn alloy is remarkable, as is shown in Fig. 18.

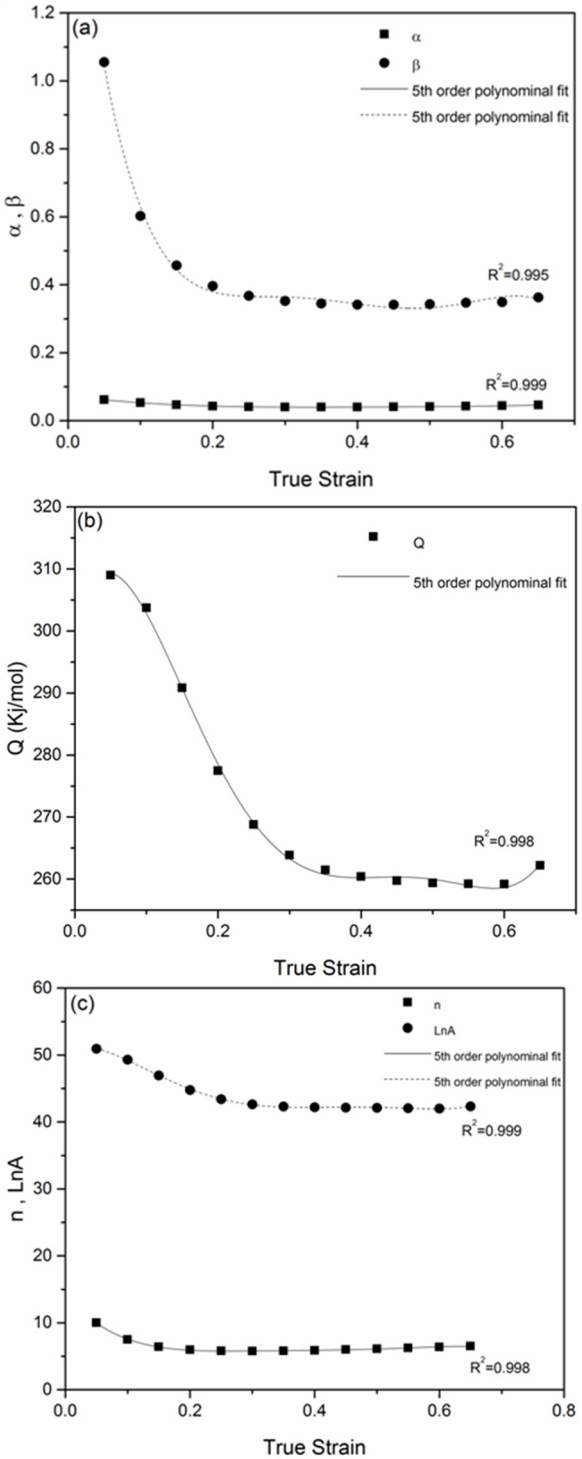

Fig. 18. Variations of (a) α, β, (b) Q and (c) n, LnA with true strain for Mg-4Sn alloy.

However, this effect is not considered in the previous constitutive model. To overcome this

[DOI: 10.22068/ijmse.2085]

drawback, material constants (β, α, n, lnA and Q) must be introduced as a function of strain to increase the accuracy of the model.

Fifth order polynomial equations were introduced to incorporate the effect of strain on the material constants at a specific strain range (0.05 - 0.65) and an interval of 0.05:

$$\beta = B_0 + B_1\varepsilon + B_2\varepsilon^2 + B_3\varepsilon^3 + B_4\varepsilon^4 + B_5\varepsilon^5$$
$$\alpha = C_0 + C_1\varepsilon + C_2\varepsilon^2 + C_3\varepsilon^3 + C_4\varepsilon^4 + C_5\varepsilon^5$$
$$n = D_0 + D_1\varepsilon + D_2\varepsilon^2 + D_3\varepsilon^3 + D_4\varepsilon^4 + D_5\varepsilon^5$$
$$LnA = E_0 + E_1\varepsilon + E_2\varepsilon^2 + E_3\varepsilon^3 + E_4\varepsilon^4 + E_5\varepsilon^5$$
$$Q = F_0 + F_1\varepsilon + F_2\varepsilon^2 + F_3\varepsilon^3 + F_4\varepsilon^4 + F_5\varepsilon^5 \quad (21)$$

The polynomial coefficients of Eq. (21) for α, β, n, lnA and Q are listed in Table 4. Using the material's constants at a given strain, Eq. (15) can be rewritten as a function of strain, and flow stress can be calculated at each strain point.

To verify the strain compensated Arrhenius type model, a comparison between the experimental and predicted flow stress of Mg-4Sn alloy at different hot deformation conditions was carried out, and is shown in Fig. 19. It is clear that unlike the J-C model, the Arrhenius model fairly well correlates with the experimental data in both the work hardening and the softening regions.

Table 4. The polynomial coefficients for α, β, n, lnA and Q for Mg-4Sn alloy

β	α	n	LnA	Q
B_0=1.842	C_0=0.074	D_0=14.29	E_0=51.30	F_0=301.93
B_1= -21.00	C_1= -0.284	D_1= -111.60	E_1= 18.58	F_1=362.96
B_2=116.07	C_2=0.809	D_2=567.81	E_2=-602.06	F_2= -5151.49
B_3= -309.39	C_3= -0.798	D_3= -1408.57	E_3= 2416.64	F_3=18783.60
B_4=394.84	C_4= -0.158	D_4=1712.43	E_4=-3748.98	F_4= -28164.90
B_5= -192.97	C_5=0.536	D_5= -810.25	E_5= 2059.07	F_5=15257.34

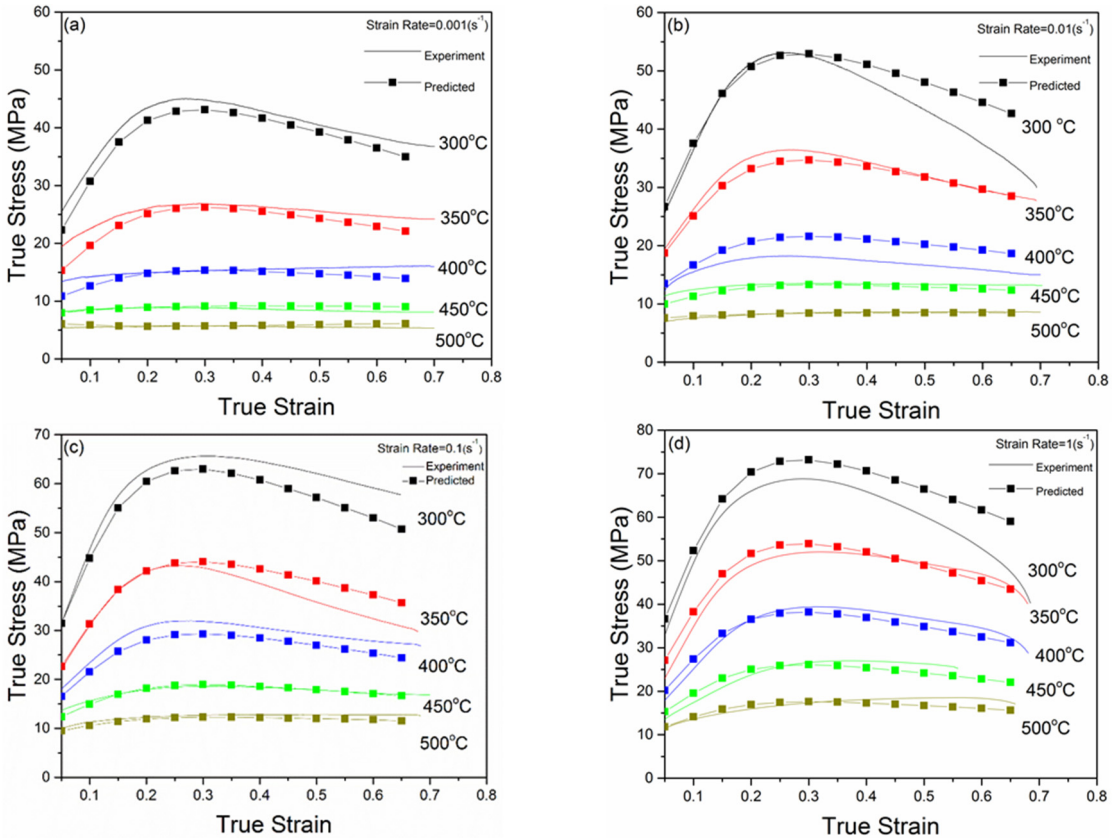

Fig. 19. Comparisons between the experimental and strain compensated Arrhenius type predicted flow stress curves of Mg-4Sn magnesium alloy at different strain rates of (a) 0.001 s^{-1}, (b) 0.01 s^{-1}, (c) 0.1 s^{-1}, (d) 1 s^{-1}.

[DOI: 10.22068/ijmse.2085]

The values of AAE and RMSE errors for the strain compensated Arrhenius type model was calculated as 5.3% and 1.7 MPa, respectively. This strongly indicates that the hyperbolic sine-type model is more accurate than the J-C, power law and exponential models to predict the hot deformation behavior of Mg-4Sn alloy.

4. CONCLUSIONS

Hot deformation behavior of Mg-4Sn ally was studied in the temperature range of 300-500°C and strain rates of 0.001-0.01 s^{-1}. A comparative study among different constitutive models for predicting of the peak stress at various deformation conditions was conducted. The following conclusions were drawn from the analysis.

- Stress-strain curves at low temperature and high strain rate showed a peak stress followed by a continuous decrease in the flow stress. However, at high temperature and low strain rate the flow stress reached a steady state.
- The peak stress predicted by the hyperbolic sine model reasonably correlated with the experimental data, RSME= 1.46 and AAE= 2.85.
- The strain-compensated Arrhenius-type constitutive equation predicted the flow curves of Mg-4Sn alloy by the minimum and the maximum errors of RSME= 0.87-2.13 and AAE= 4.07-6.64, respectively.

REFERENCES

[1] Sadeghi, M., Hadi, M., Bayat, O. and Karimi, H., "Hot deformation of the Mn-Ni-Cr alloy during compression", Iran. J. Mater. Sci. Eng., 2020, 17, 102-108.

[2] Cheng, W.L., Tian, Q.W., Yu, H., Zhang, H. and You, B.S., "Strengthening mechanisms of indirect-extruded Mg–Sn based alloys at room temperature", J. Mag. Alloys, 2014, 2, 299-304.

[3] Mortezaei, S., Arabi, H., Seyedein, H., Momeny, A. and Soltanalinezhad, M., "Investigation on microstructure evolution of a semi-austenitic stainless steel through hot deformation", Iran. J. Mater. Sci. Eng., 2020, 17, 60-69.

[4] Massalski, T.B., Okamoto, H., Subramanian, P. and Kacprzak, L., Binary alloy phase diagrams, vol. 3, ASM International, 1990, 1485.

[5] Liu, H., Chen, Y., Tang, Y., Wei, S. and Niu, G., "The microstructure, tensile properties, and creep behavior of as-cast Mg–(1–10)% Sn alloys", J. Alloys Comp., 2007, 440, 122-126.

[6] Nie, J.F., "Precipitation and hardening in magnesium alloys", Metall. Mater. Trans. A, 2012, 43, 3891-3939.

[7] Mosadegh, S., Aghaie-Khafri, M. and Binesh, B., "Microstructural evolution and flow behaviour in hot compression of as-extruded Mg–Gd–Nd–Zn–Zr alloy", Phil. Mag., 2021, 101, 2473-2501.

[8] Salari, O., Abdi, A., and Aghaie-Khafri, M., "A New Criterion for Construction of Instability Maps in Hot Deformation", Mater. Perform. Charact., 2019, 8, 856-858.

[9] Kim, D.H., Lee, J.Y., Lim, H.K., Kyeong, J.S., Kim, W.T. and Kim, D.H., "The effect of microstructure evolution on the elevated temperature mechanical properties in Mg-Sn-Ca system", Mater. Trans., 2008, 49, 2405-2413.

[10] Luo, X., Kang, L., Li, Q. and Chai, Y., "Microstructure and hot compression deformation of the as-cast Mg–5.0 Sn–1.5 Y–0.1 Zr alloy", App. Phys. A, 2015, 120, 699-705.

[11] Dieter, G.E., Workability testing techniques, American Society for Metals, Ohio, USA, 1984.

[12] Ebrahimi, R. and Najafizadeh, A., "A new method for evaluation of friction in bulk metal forming", J. Mater. Process. Technol., 2004, 152, 136-143.

[13] Wei, G., Peng, X., Hu, F., Hadadzadeh, A., Yan, Y., Xie, W. and Wells, M.A., "Deformation behavior and constitutive model for dual-phase Mg–Li alloy at elevated temperatures", Trans. Nonferr. Metal Soc., 2016, 26, 508-518.

[14] Honarmandi, P., Aghaie-Khafri, M., "Hot deformation behavior of Ti–6Al–4V alloy in β phase field and low strain rate", Metallogr. Microstruct. Anal., 2013, 2, 13-20.

[15] Rao, K., Prasad, Y., Hort, N. and Kainer, K., "Hot workability characteristics of cast and homogenized Mg–3Sn–1Ca alloy", J. Mater. Process. Technol., 2008, 201, 359-

[DOI: 10.22068/ijmse.2085]

363.
[16] Mosadegh, S., Aghaie-Khafri, M. and Binesh, B., "Hot Workability and Processing Map of High Gd Content Mg-Gd-Zn-Zr-Nd Alloy", Iran. J. Mater. Form., 2021, 8, 44-53.
[17] Tan, C.W., Xu, S., Lu, W., Chen, Z.Y., Wang, F. and Cai, H., "Effect of temperature on mechanical behavior of AZ31 magnesium alloy", Trans. Nonferr. Metal. Soc., 2007, 17, 41-45.
[18] Zhu, Y., To, S., Lee, W., Liu, X., Jiang, Y. and Tang, G., "Effects of dynamic electropulsing on microstructure and elongation of a Zn–Al alloy", Mater. Sci. Eng. A, 2009, 501, 125-132.
[19] Yan, L.m., Shen, J., Li, J., Li, Z. and Yan, X., "Deformation behavior and microstructure of an Al-Zn-Mg-Cu-Zr alloy during hot deformation", Int. J. Miner. Metall. Mater., 2010, 17, 46-52.
[20] Wang, Y., Peng, J., Zhong, L. and Pan, F., "Modeling and application of constitutive model considering the compensation of strain during hot deformation", J. Alloys Compd., 2016, 681, 455-470.
[21] Lin, Y. and Chen, X., "A critical review of experimental results and constitutive descriptions for metals and alloys in hot working", Mater Des., 2011, 32, 1733-1759.
[22] Shin, H. and Kim, J., "A phenomenological constitutive equation to describe various flow stress behaviors of materials in wide strain rate and temperature regimes", J. Eng. Mater. Technol., 2010, 132, 1-5.
[23] Rusinek, A., Rodríguez-Martínez, J.A. and Arias, A., "A thermo-viscoplastic constitutive model for FCC metals with application to OFHC copper", Int. J. Mech. Sci., 2010, 52, 120-135.
[24] Johnson, G.R. and Cook, W.H., "A constitutive model and data for metals subjected to large strains, high strain rates and high temperatures", Proceedings of the 7th International Symposium on Ballistics, The Hague, The Netherlands, 1983, 541-547.
[25] Duc-Toan, N., Tien-Long, B., Dong-Won, J., Seung-Han, Y. and Young-Suk, K., "A modified Johnson–Cook model to predict stress-strain curves of boron steel sheets at elevated and cooling temperatures", High Temp. Mater. Proc., 2012, 31, 37-45.
[26] Lin, Li, Y. L.T., Fu, Y.X. and Jiang, Y.Q., "Hot compressive deformation behavior of 7075 Al alloy under elevated temperature", J. Mater. Sci., 2012, 47, 1306-1318.
[27] Lin, Y., Li, Q.F., Xia, Y.C. and Li, L.T., "A phenomenological constitutive model for high temperature flow stress prediction of Al–Cu–Mg alloy", Mater. Sci. Eng. A, 2012, 534, 654-662.
[28] Roy, M., Maijer, D. and Dancoine, L., "Constitutive behavior of as-cast A356", Mater. Sci. Eng. A, 2012, 548, 195-205.
[29] Momeni, A., Abbasi, S.M. and Sadeghpour, S., "A comparative study on the hot deformation behavior of $Ti_5Al_5Mo_5V_3Cr$ and newly developed $Ti_4Al_7Mo_3V_3Cr$ alloys", Vacuum, 2019, 161, 410-418.
[30] Samantaray, D., Mandal, S. and Bhaduri, A., "A comparative study on Johnson Cook, modified Zerilli–Armstrong and Arrhenius-type constitutive models to predict elevated temperature flow behaviour in modified 9Cr–1Mo steel", Comp. Mater. Sci., 2009, 47, 568-576.
[31] Li, H.Y., Wang, X.F., Duan, J.Y. and Liu, J.J., "A modified Johnson Cook model for elevated temperature flow behavior of T24 steel", Mater. Sci. Eng. A, 2013, 577, 138-146.
[32] He, A., Xie, G., Zhang, H. and Wang, X., "A comparative study on Johnson–Cook, modified Johnson–Cook and Arrhenius-type constitutive models to predict the high temperature flow stress in 20CrMo alloy steel", Mater. Des., 2013, 52, 677-685.
[33] Abbasi-Bani, A., Zarei-Hanzaki, A., Pishbin, M. and Haghdadi, N., "A comparative study on the capability of Johnson–Cook and Arrhenius-type constitutive equations to describe the flow behavior of Mg–6Al–1Zn alloy", Mechanics of Materials 71 (2014) 52-61.
[34] Zener, C. and Hollomon, J.H., "Effect of strain rate upon plastic flow of steel", J. of App. Phys., 2009, 15, 22-32.
[35] Frost, H.J., and Ashby, M.F., Deformation-mechanism maps: the plasticity and creep of metals and ceramics, Pergamon Press, 1982.

[DOI: 10.22068/ijmse.2085]

[36] Slooff, F., Zhou, J., Duszczyk, J. and Katgerman, L., "Constitutive analysis of wrought magnesium alloy Mg–Al4–Zn1", Scr. Mater., 2007, 57, 759-762.
[37] Mirzadeh, H., "Constitutive modeling and prediction of hot deformation flow stress under dynamic recrystallization conditions", Mech. Mater., 2015, 85, 66-79.
[38] Cai, Z., Chen, F. and Guo, J., "Constitutive model for elevated temperature flow stress of AZ41M magnesium alloy considering the compensation of strain", J. Alloys Comp., 2015, 648, 215-222.
[39] Sun, Z., Li, Y., Zhang, K., Li, X., Ma, M., Shi, G., Yuan, J. and Zhang, H., "Microstructure and Hot Deformation Behavior of the Mg–8 wt.% Sn–1.5 wt.% Al Alloy", Materials, 2021, 12, 2050.
[40] Rao, K.P., Prasad, Y.V.R.K., Suresh, K., Hort, N. and Kainer, K.U., "Hot deformation behavior of Mg-2Sn-2Ca alloy in as-cast condition and after homogenization", Mater. Sci. Eng. A, 2012, 552, 444-450.
[41] K. Suresh, K.P. Rao, Y.V.R.K. Prasad, N. Hort and K.U. Kainer, "Investigation of hot workability behavior of as-cast Mg–5Sn–2Ca (TX52) magnesium alloy through processing map", Prod. Manuf. Res., 2014, 2, 241-252.

[DOI: 10.22068/ijmse.2085]